

# The lysine- and glutamic acid-rich protein KERP1 plays a role in *Entamoeba histolytica* liver abscess pathogenesis

Julien Santi-Rocca,<sup>1,2†</sup> Christian Weber,<sup>1,2†</sup>

Ghislaine Guigon,<sup>3</sup> Odile Sismeiro,<sup>3</sup>

Jean-Yves Coppée<sup>3</sup> and Nancy Guillén<sup>1,2\*</sup>

<sup>1</sup>Institut Pasteur, Unité Biologie Cellulaire du Parasitisme, Paris, F-75015, France.

<sup>2</sup>INSERM U786, Paris, F-75015, France.

<sup>3</sup>Institut Pasteur, Genopole@ Ile-de-France, Paris, F-75015, France.

## Summary

The parasite *Entamoeba histolytica* colonizes the large bowel where it may persist as an asymptomatic luminal gut infection, which changes to virulence. Parasite invasion of the intestine leads to dysentery and spreads to the liver, where amoebae form abscesses. We took advantage of changes in virulence that occurs after long-term *in vitro* culture of *E. histolytica* strains. Using microarrays, we concluded that virulence correlates with upregulation of key genes involved in stress response, including molecular chaperones, *ssp1* and peroxiredoxin; as well as the induction of unknown genes encoding lysine-rich proteins. Seven of these were retained with respect to their lysine content higher than 25%. Among them, we found KERP1, formerly identified as associated to parasite surface and involved in the parasite adherence to host cells. Experimentally induced liver abscesses, using molecular beacons and protein analysis, allowed us to draw a parallel between the intricate upregulation of *kerp1* gene expression during abscess development and the increased abundance of KERP1 in virulent trophozoites. Following its characterization as a marker for the progression of infection, KERP1 was also seen to be a virulence marker as trophozoites affected in *kerp1* expression by an antisense strategy were unable to form liver abscesses.

## Introduction

*Entamoeba histolytica* is a human pathogen that causes amoebiasis, the third leading parasitic cause of death worldwide. *E. histolytica* infection is most prevalent in the poorest regions of the world, as is the case for most infectious diseases. The parasite has a simple two-stage life cycle, existing either as cysts (the contamination form) or as vegetative, amoeboid trophozoites (Stanley, 2003). After cyst ingestion by way of faeces-contaminated food or water, excystation takes place in the lumen of the small intestine. Motile trophozoites then move to and colonize the colon. The majority of human *E. histolytica* infections remain asymptomatic. However, in some cases, infectious trophozoites penetrate the intestinal mucosa and disseminate to other organs (most commonly the liver), where they induce abscess formation. The parasite and host factors determining the outcome of symptomatic infection (rather than commensal colonization) are not known yet. Pathophysiological analyses of amoebiasis have shown that trophozoite virulence relies on specific cellular and molecular interactions between parasites and human cells (Stanley, 2003). These include: adhesion via a galactose (Gal) and *N*-acetyl-D-galactosamine (GalNAc)-specific lectin (Petri *et al.*, 2002), disruption of mucosal barriers by amoebic proteinases (Lidell *et al.*, 2006) and lysis of epithelial and inflammatory cells by pore-forming proteins (Leippe, 1997), phospholipases (Ravdin *et al.*, 1985) and haemolytic factors (Said-Fernandez and Lopez-Revilla, 1988), leading to colonic ulcers and tissue invasion. In turn, infection triggers a host cellular and immune response. Evidence for the involvement of the immune system includes the presence of an inflammatory infiltrate (i.e. higher numbers of lymphocytes, macrophages and neutrophils) in the intestinal mucosa (Seydel *et al.*, 1998) and in granulomas during liver abscess formation (Tsutsumi *et al.*, 1984). The host employs both innate and adaptive immune responses to protect itself from *E. histolytica* (Salata and Ravdin, 1986; Asgharpour *et al.*, 2005). These environmental changes (which are often detrimental to the pathogen) are generally considered as stress conditions. For instance, cytokine release by immune effector cells can lead to temperature fluxes that may influence the parasite's

Received 6 April, 2007; revised 11 July, 2007; accepted 17 July, 2007. \*For correspondence. E-mail nguillen@pasteur.fr; Tel. (+33) 1 45 68 86 75; Fax (+33) 1 45 68 86 74. †These two authors contributed equally to this work.

ability to maintain itself in the host tissue. However, *E. histolytica*'s ability to survive during infection by resisting the host's immunological responses testifies its use of strategies to escape them.

Hepatic amoebiasis can be studied by using a model of abscess formation in hamsters (Tsutsumi *et al.*, 1984). It is noteworthy that trophozoites purified from abscesses lose their virulence when multiplied extensively in axenic culture; regular passage into hamster livers is required for virulence preservation. The parasite's ability to switch from asymptomatic colonization to invasive infection and the need for exacerbated virulence in animals suggest the existence of fine-tuned mechanisms for adaptation to growth in different milieus. Understanding the reprogramming of gene expression in *E. histolytica* following environmental changes should thus provide clues about the molecular mechanisms sustaining cell survival, in particular during infection.

The complete genome sequence of *E. histolytica* has been published (Loftus *et al.*, 2005), providing new opportunities for the examination of gene expression profiles in parasites subjected to modified life conditions. Genome and transcriptome analyses of *E. histolytica* avirulent isolates (Davis *et al.*, 2006; MacFarlane and Singh, 2006) have thus shown that their attenuated virulence correlates with divergences at the genetical and transcriptional levels when compared with virulent trophozoites. To identify gene expression changes that may be associated with parasite environmental adaptation and survival during infection, we used a transcript-based microarray technology (Weber *et al.*, 2006). We characterized the expression of 1130 *E. histolytica* genes at the RNA level in trophozoites from the same genetic background. We compared the transcriptional profiles of highly virulent parasites with those of trophozoites from the same strain but which had lost the capacity to form liver abscesses (following long-term axenic culture). Our data showed that parasites freshly isolated from an abscess display an enhanced stress response. In addition to stress-response, transcription-regulation and cytoskeleton-related genes, a group of genes encoding lysine-rich proteins with unknown functions were also upregulated in virulent trophozoites. Seven of them were highlighted by the high lysine content (more than 25%) of the proteins they potentially encode. Of these, particularly prominent was the gene encoding KERP1, a lysine- and glutamic acid-rich protein that we have previously shown to be involved in the interaction of *E. histolytica* with human cells (Seigneur *et al.*, 2005). Further analyses (using experimentally induced amoebiasis in hamsters) enabled us to investigate the link between *kerp1* gene overexpression and hepatic amoebiasis; we detected a particular change in *kerp1* gene expression on the third day of infection. The upregulation of *kerp1* gene expres-

sion and cortical KERP1 progressive accumulation in parasites were observed within the inflammatory foci, whereas a reduction in protein abundance progressively occurred during axenic growth of *E. histolytica*, which correlates with the decrease of virulence. The use of anti-sense RNA-mediated inhibition of *kerp1* gene expression suggested an intricate gene regulation, which led under stress conditions to a reduction of KERP1 abundance, correlated with the reduced ability of modified trophozoites to provoke liver abscesses. From these data, we concluded that KERP1 is a key parasite factor for the establishment and progress of liver abscesses and, consequently, for amoebic virulence.

## Results

The initial objective of this work was to define general patterns of gene expression in an *E. histolytica* strain displaying different levels of virulence (i.e. its ability to induce liver abscesses). To this end, the HM1:IMSS strain of *E. histolytica* was inoculated into hamsters, with parasites then being harvested from liver abscesses after 7 days. We compared gene expression profiles for virulent parasites and for trophozoites from the same strain but which had lost the capacity to develop abscesses after being axenically cultured for more than 3 years. To monitor changes in RNA abundance, we performed quantitative analysis of the RNA populations from virulent and non-virulent parasites by using a home-made oligonucleotide microarray carrying information obtained directly from sequence analysis of *E. histolytica* transcripts – a strategy that is generally acknowledged as overcoming problems which may arise from alternative intron splicing and gene redundancy. The data from three biological replicates were analysed, normalized and raw *P*-values adjusted (see *Experimental procedures*). Presented in this analysis are only genes with a fold change more than 2 and a significant associated *P*-value (less than 0.05). In Tables S2 and S3, listed are all genes presenting expression modulation with a significant *P*-value regardless of the fold change. The totality of results and details are in addition available online in the genoscript database (<http://genoscript.pasteur.fr>).

### Overview of genes modulated in virulent trophozoites

The overall expression analysis identified both hypothetical and characterized *E. histolytica* genes that may contribute to adaptation to survival in axenic culture such as metabolism-, protein synthesis- and signal transduction-related genes. Transcriptional profiling of virulent trophozoites showed that 21 genes were downregulated, among which two genes deserved particular attention, as they were strongly repressed. The first gene (XM\_649962) was

**Table 1A.** Genes upregulated in virulent parasites.

Oligonucleotide ID	Gene identification at NCBI <sup>a</sup>		Description	FC	P-value
Cell growth, division and DNA synthesis					
EH-IP0902	70.t00027	XM_648747	S-adenosylmethionine synthetase	2.5	1.47E-04
Cell rescue, defence, senescence and death					
EH-IP0368	216.t00010	XM_645403	Ehssp1	9.2	2.41E-12
EH-IP0715	442.t00004	XM_643430	Peroxiredoxin	2.2	3.50E-05
EH-IP0160	136.t00007	XM_646911	Peroxiredoxin	2.1	4.15E-02
EH-IP1002	963.t00001	XM_642754	Peroxiredoxin	2.1	2.87E-02
Cellular organization/biogenesis					
EH-IP0375	22.t00027	XM_650730	Villin-related protein	2.3	6.72E-03
EH-IP0815	56.t00006	XM_649253	Calcium-binding protein 1	2.3	8.72E-04
EH-IP0764.4	5.t00037	XM_651936	Myosin heavy chain	2.2	7.74E-03
EH-IP0672	4.t00117	XM_651988	Calcium-binding protein 2	2.1	6.04E-03
Energy generation					
EH-IP0439	26.t00021	XM_650509	Malate dehydrogenase	3.4	1.02E-09
Hypothetical					
EH-IP0761	5.t00017	XM_651968	Hypothetical	3.1	4.62E-06
EH-IP0807.2	54.t00042	XM_649330	Hypothetical	2.7	5.77E-05
EH-IP0267	182.t00019	XM_646028	Hypothetical	2.6	3.88E-07
EH-IP0920	77.t00030	XM_648537	Hypothetical	2.5	3.88E-05
EH-IP0598	34.t00038	XM_650092	Hypothetical	2.4	8.61E-08
EH-IP0825	59.t00004	XM_649122	Hypothetical	2.4	9.61E-04
EH-IP0213	16.t00040	XM_651115	Hypothetical	2.3	1.06E-02
EH-IP0821.1	58.t00022	XM_649180	Hypothetical	2.3	5.04E-03
EH-IP0821.4	58.t00022	XM_649180	Hypothetical	2.2	1.08E-02
EH-IP0821.1	58.t00022	XM_649180	Hypothetical	2.2	1.21E-02
EH-IP0353.1	21.t00051	XM_650801	Hypothetical	2.2	1.70E-02
EH-IP0913.2	76.t00003	XM_648547	Hypothetical	2.1	1.13E-03
EH-IP0821.6	58.t00022	XM_649180	Hypothetical	2.1	2.30E-02
EH-IP1014	99.t00020	XM_647855	Hypothetical	2.0	3.12E-03
EH-IP0913.1	76.t00003	XM_648547	Hypothetical	2.0	3.21E-03
Metabolism					
EH-IP0399	233.t00003	XM_645150	Iron hydrogenase	2.1	7.45E-04
Protein synthesis and destination					
EH-IP0718	444.t00002	XM_643416	60S ribosomal protein L29	2.3	3.21E-03
EH-IP0876	64.t00032	XM_648974	Ubiquitin	2.2	1.77E-05
Transcription and RNA processing					
EH-IP0315	2.t00072	XM_652289	RNA-binding protein	2.5	8.81E-05
EH-IP0890	69.t00022	XM_648786	Transcriptional co-activator	2.2	3.90E-04
Virulence					
EH-IP0216	160.t00008	XM_646438	Surface antigen ariel1	3.3	2.43E-07
EH-IP0334.2	202.t00007	XM_645632	20 kDa antigen-related	2.0	1.32E-05
Unclassified					
EH-IP1127	gDNA_group24		Unknown	2.1	6.38E-03

a. <http://www.ncbi.nlm.nih.gov/gquery/gquery.fcgi?term=ENTAMOEBA>

Information from sequenced transcripts present in cultured virulent *Entamoeba histolytica* allowed for the design of 70 bases oligonucleotides spotted in the microarray. The complete data set and detailed analyses are available at <http://genoscript.pasteur.fr> and in Tables S2 and S3. Listed in this table are the annotated genes that undergo at least twofold upregulation in virulent trophozoites.

repressed 22.7-fold and encodes a protein presenting homologies with the dilute domain encountered in Class V unconventional myosin and whose function is unknown. The protein does not bear any other classic myosin-specific domains, indicating that further experiments should be performed in order to assess whether this protein belongs to the unconventional myosin family (i.e. by investigating its capacity to hydrolyse ATP and to bind actin filaments). The second gene (XM\_645291) encodes a protein sharing 40% homology with the protein encoded by XM\_649962; in addition, it presents a spectrin repeat domain. Future experimental studies will elucidate the role of these cytoskeleton related factors found

downregulated. We then focused the analysis on the 29 genes that were upregulated (Table 1) in virulent parasites. Surprisingly, expression of many of the genes known as virulence-related were not changed in virulent trophozoites at the exception of the asparagine-rich protein ARIEL (Mai and Samuelson, 1998) and the 20 kDa factor (Zhang and Samuelson, 1993). Genes encoding stress-related proteins were among the most highly expressed ones. Noteworthy findings included the nine-fold overexpression of the *ssp1* stress-inducible gene (Satish *et al.*, 2003), peroxiredoxin (providing protection from oxidative stress) and, very close to scores, two isoforms of Hsp90 (an important chaperone in the stress

**Table 1B.** Gene expression determined by qRT-PCR in virulent trophozoites.

Gene name	Accession number at NCBI <sup>a</sup>	Fold change $\pm$ SD
<i>ariel</i>	XM_646438	3.67 $\pm$ 0.26
<i>krip3</i>	XM_649180	2.67 $\pm$ 1.03
<i>krip2</i>	XM_650801	1.98 $\pm$ 0.60
<i>kerp1</i>	XM_648537	2.40 $\pm$ 0.42

a. <http://www.ncbi.nlm.nih.gov/gquery/gquery.fcgi?term=ENTAMOEB>

*ariel*, *krip2*, *krip3* and *kerp1* gene expression was assessed by qRT-PCR, normalized with respect to the abundance of *L9* mRNA and reported to the values obtained with avirulent trophozoites. Data are means of results  $\pm$  standard deviation obtained with two different matrix dilutions for two independent experiments ( $n = 4$ ) quantified in triplicate wells.

response). Genes involved in the ubiquitin-dependent proteolysis pathway and those encoding 26S proteasome regulatory complex components were also upregulated in virulent parasites.

One major feature was found by a careful computational analysis of upregulated genes encoding proteins of unknown functions: seven genes encoding proteins car-

rying high lysine content (over 25%). These were identified and were referred to as KRiPs, for 'lysine-rich proteins' (Table 2). Two *krip* genes (*krip2* and *krip3*) along with two others (*krip1* and *krip4*) that appeared in the statistical analysis with a fold change close to the threshold were upregulated in virulent parasite; two of the hypothetical proteins (KRiP2 and KRiP3) share 47% identity

**Table 2.** Hypothetical protein-encoding genes modulated in virulent parasites.

A. Identification of domains of interest in hypothetical proteins.

Gene identification at NCBI <sup>a</sup>	FC	Domain of interest at the protein level <sup>b</sup>	
Upregulated			
5.t00017	XM_651968	3.1	NO HITS
54.t00042	XM_649330	2.7	Vinculin/catenin
182.t00019	XM_646028	2.6	Mnd1 (meiotic nuclear division 1)
77.t00030	XM_648537	2.5	NO HITS
34.t00038	XM_650092	2.4	DEK protein
59.t00004	XM_649122	2.4	Signal peptide
16.t00040	XM_651115	2.3	Signal peptide
58.t00022	XM_649180	2.3	Signal peptide
21.t00051	XM_650801	2.2	Histone H5
76.t00003	XM_648547	2.1	DEK protein
99.t00020	XM_647855	2.0	NO HITS
Downregulated			
37.t00023	XM_649962	22.7	Dilute (myosin V)
223.t00011	XM_645291	7.9	Ribosomal L11/dilute/spectrin
108.t00018	XM_647622	4.3	Signal peptide/transmembrane regions
21.t00007	XM_650804	2.8	Transmembrane regions
328.t00002	XM_644144	2.3	Signal peptide
195.t00004	XM_645775	2.1	PT repeat (XPTX tetrapeptide repeats)
35.t00013	XM_650073	2.0	NO HITS

B. Characteristics of lysine-rich proteins whose genes are upregulated in virulent parasites.

Name	Accession number at NCBI <sup>a</sup>	Lysine (%)	Glutamic acid (%)	Molecular mass (kDa)	Purified with phagosomes <sup>c</sup>	
KRiP1	XP_656911	XM_651819	28.9	6.4	60	No
KRiP2	XP_655893	XM_650801	34.3	3.8	94	Yes
KRiP3	XP_654272	XM_649180	34.6	7.3	95	Yes
KRiP4	XP_656912	XM_651820	29.2	2.8	51	No
KERP1	XP_653629	XM_648537	25	19	22	Yes
KERP2	XP_653639	XM_648547	25.5	14	28	Yes
KERP3	XP_655184	XM_650092	24.9	14.5	28	No

Listed are hypothetical protein-encoding genes that undergo at least twofold modulation in virulent trophozoites (A). The indicated hypothetical proteins correspond to lysine-rich proteins (KRiPs) and lysine- and glutamic acid-rich proteins (KERPs) that are significantly modulated in virulent trophozoites (B), highlighting a lysine content more than 24% for both groups, and a glutamic acid abundance higher than 14% for KERPs. Some proteins were also identified by proteomic analysis after phagosome purification (Marion *et al.*, 2005).

a. <http://www.ncbi.nlm.nih.gov/gquery/gquery.fcgi?term=ENTAMOEB>

b. Obtained by searching at InterProScan data base.

c. Identified by proteomic analysis (Marion *et al.*, 2005).

and feature a potential, cleavable signal peptide. Among KRiP factors, a subfamily characterized by a high glutamic acid content (over 14%) was referred to as 'lysine- and glutamic acid-rich proteins' (KERPs). Two of the upregulated genes were *kerp1* and *kerp2*, which we had previously identified as encoding important parasite surface factors with affinity for human cells (Seigneur *et al.*, 2005) and as being enriched in phagosome fractions of *E. histolytica* (Marion *et al.*, 2005). The microarray analysis performed here enabled us to identify another *kerp* gene (*kerp3*, Accession No. 34.t00038) encoding a protein that shares 62% identity (by amino acids sequence alignment) with KERP2. Although *kerp2* and *kerp3* are classified in the same group and are both upregulated in virulent trophozoites, the two genes encode proteins that differ significantly from KERP1. None of the three identified KERPs possesses either a translocation signal peptide or a known consensus sequence for compartment localization or retention. By quantitative real-time polymerase chain reaction (qRT-PCR), we confirmed that *krip2* and *krip3* (as well as *ariel* and *kerp1*) (Table 1B) were upregulated in virulent parasites, when compared with long-term cultured trophozoites.

#### *kerp1* gene expression profile during liver infection using molecular beacon-based qRT-PCR

The present microarray analysis of relative transcript amounts in virulent parasites suggested that, in addition to the classic stress response genes, several other genes (such as *kerp1*) may be important for virulence in *E. histolytica*. We decided to test this hypothesis by a further characterization of *kerp1* gene expression during infection with the aim of, first, analysing the role of KERP1 in pathogenicity and, second, providing a biological reach to our microarray discoveries. To determine whether enhanced levels of mRNAs in virulent parasites corresponded to changes in gene expression during infection, we specifically quantified *kerp1* mRNA at different stages of liver abscess development using qRT-PCR with molecular beacons.

If molecular beacons are to be used in qRT-PCR experiments as highly specific and sensitive probes, they must exhibit hybridization at an appropriate temperature and high target sensitivity (Tyagi and Kramer, 1996). We undertook to quantify *kerp1* mRNA and in parallel, for data normalization purposes, this coding for the L9 ribosomal protein (whose abundance was determined as invariant by microarray analysis and by qRT-PCR as compared with L31 ribosomal protein-encoding gene). We checked the assay's characteristics by measuring the fluorescence emitted after hybridization of these probes (*kerp1*-MB and L9-MB) with either their proper targets or irrelevant

targets. The fluorescence data obtained following hybridization of each molecular beacon (Fig. 1A and B) showed that the choice of 55°C for hybridization during the PCR was appropriate, as it allowed specific hybridization of primers and efficient target detection.

In order to study the kinetics of *kerp1* gene expression during liver abscess development, hamsters were sacrificed 2, 3, 4 and 5 days after infection with virulent HM1:IMSS trophozoites. The *kerp1*/L9 mRNA ratio (determined by qRT-PCR) for amoebae within inflammatory foci was compared with the ratio obtained with virulent trophozoites growing in axenic culture. The data (Fig. 1C) showed a drop in *kerp1* mRNA levels early in the infective process (with decreases of  $24.8 \pm 19.7\%$  and  $50.6 \pm 19.5\%$  on the second and third days of infection respectively). Four days after parasite inoculation, *kerp1* gene expression rose to  $78.6 \pm 28.6\%$  of its initial value and overtook the baseline value ( $112 \pm 24.9\%$ ) on the fifth day of infection. A one-way analysis of variance (ANOVA) indicated that *kerp1* gene expression was significantly modulated during the course of hepatic infection in the hamster model we used ( $P = 0.0257$ ).

#### Quantification of KERP1 during liver infection and axenic culture of trophozoites

To determine whether the greater mRNA abundance identified by microarray and qRT-PCR analyses resulted in a corresponding increase in the amount of gene product, KERP1 protein was measured immunohistologically in hepatic abscesses and in cultured virulent and non-virulent parasites.

One day after infection, KERP1 labelling inside the trophozoites was weak and homogeneously dispersed throughout the cell (Fig. 2). On the second day post infection, the intensity of KERP1 staining increased slightly and was preferentially located in the parasites' cortical regions. Three days after trophozoite injection, KERP1 labelling was pronounced and its patchy, cortical localization was accentuated. At 5 days post infection, the plasma membrane was intensely stained right around the amoebae, although KERP1 could still be detected in the cytoplasm. Data from this experiment demonstrated the preferential localization of KERP1 in the trophozoite's cortical areas and also highlighted the intricate regulation of KERP1 levels around 3 days after parasite inoculation into hamsters.

In order to describe changes over time in the amount of KERP1 in trophozoites during axenic culture, total-protein extracts were obtained from virulent trophozoites that were cultured (after harvesting from liver abscesses) for different periods of time (i.e. 1 week and 1 month), as well as from trophozoites of the same strain that had lost their ability to induce liver abscesses in hamsters following

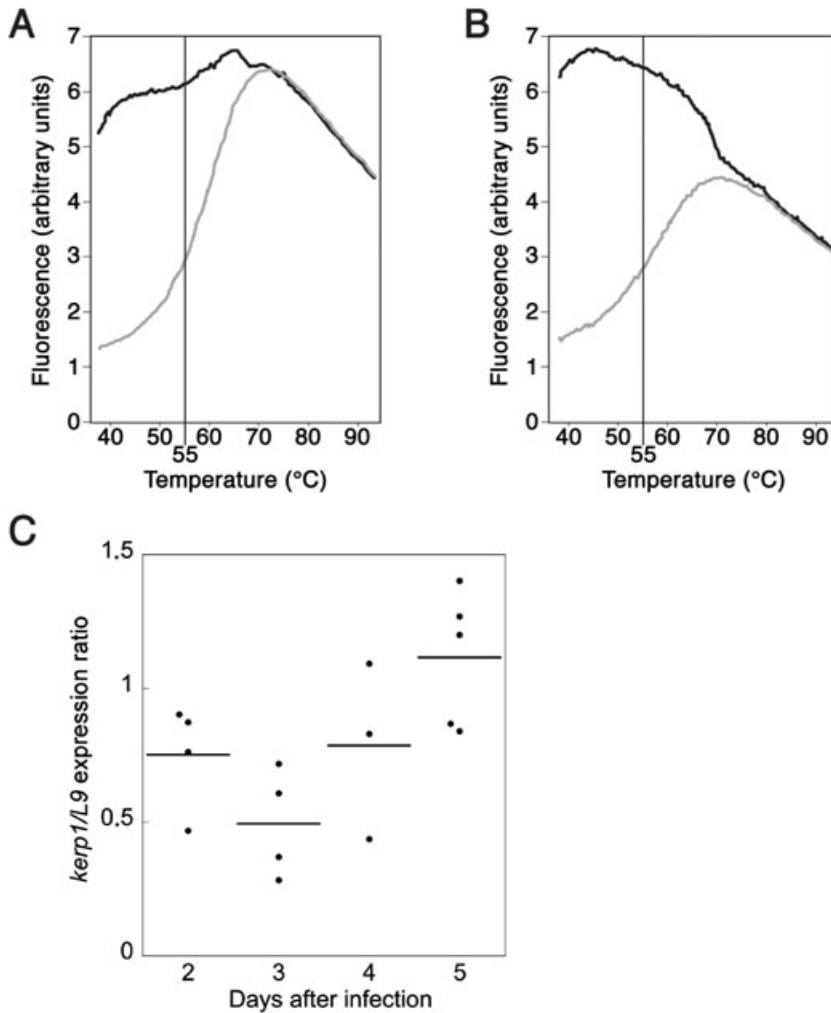


**Fig. 1.** *kerp1* gene expression during liver abscess formation.

A and B. *In vitro* validation of molecular beacon assays. *kerp1* (A) and *L9* (B) molecular beacons were incubated with their proper targets (black curves) or irrelevant targets (grey curves), as described in *Experimental procedures*. The vertical line represents the temperature (55°C) at which fluorescence emission was measured during the qRT-PCR experiments, allowing discrimination between background and signal.

C. Two to five days after infection with  $10^6$  HM1:IMSS trophozoites, animals were sacrificed and liver tissues prepared for retrotranscription. *kerp1* gene expression was quantified by qRT-PCR using molecular beacons and normalized with respect to the abundance of *L9* mRNA. Each dot represents the results obtained for one animal, relative to those raised with virulent trophozoites in axenic culture. Horizontal bars represent the mean value of *kerp1* gene expression at each time point. Data are the means of triplicate experiments, with two matrix dilutions performed in two independent quantifications ( $n = 4$ ). Analysis of variance (ANOVA) confirmed that *kerp1* gene expression was significantly modulated during the course of infection ( $P = 0.0257$ ).

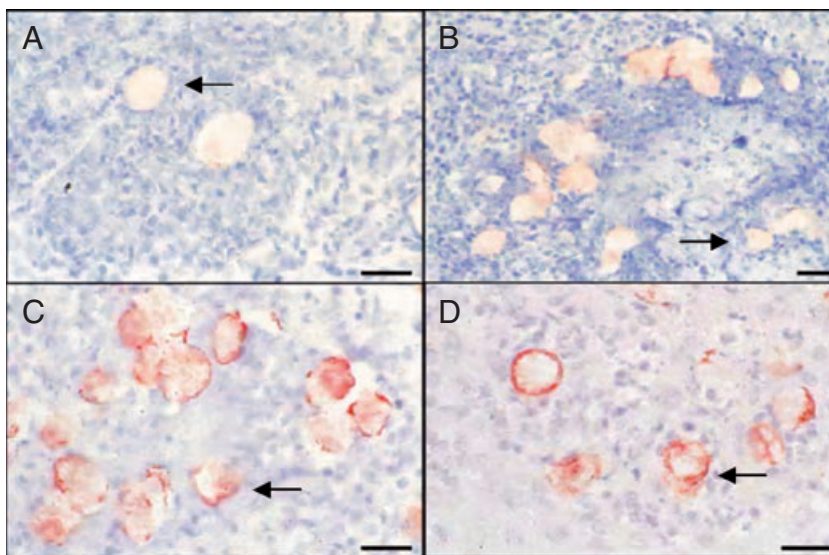


**Fig. 2.** Histoimmunochemical detection of KERP1 in hamster liver abscesses. Tissue sections were recovered from infected animals at different time points post infection: (A) 1 day, (B) 2 days, (C) 3 days and (D) 5 days. Hepatocyte and inflammatory cell nuclei were revealed by haematoxylin staining (blue). Trophozoites (arrows) were detected by a KERP1-specific polyclonal antibody (red). During the formation of liver abscesses, KERP1 appeared localized close to cortical areas and was detected in greater amounts. Scale bars, 20  $\mu$ m.

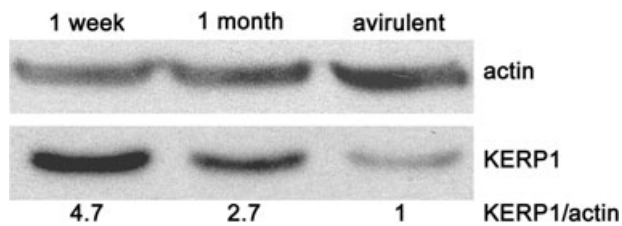


**Fig. 3.** Immunodetection of KERP1 in trophozoites in axenic culture. After culturing virulent parasites (for 1 week or 1 month) isolated from infected livers, crude trophozoite protein extracts underwent Western blot analysis in order to quantify KERP1 (25 kDa). Trophozoites that had lost virulence properties were also tested. Equivalent amounts of trophozoites ( $4 \times 10^4$ ) were loaded for each condition. The data were normalized by immunoquantification of actin (43 kDa) on the same blot according to *Experimental procedures* and taking the ratio KERP1/actin in non-virulent parasites as reference equal to 1. The detected amount of KERP1 decreased following the growth of parasites in axenic conditions. Similar results were obtained in three independent experiments.

long-term axenic culture (Fig. 3). Total protein extracts were resolved by electrophoresis and the relative abundance of KERP1 was determined by immunoblotting. The detected quantity of KERP1 in virulent trophozoites decreased along axenic culture and was higher than in avirulent ones. After data normalization, we found that the quantity of KERP1 decreased by a factor of 1.8 after 1 month of axenic culture and 4.7-fold in avirulent trophozoites, when compared with trophozoites cultured axenically for 1 week.

#### *Modification of KERP1 protein abundance by antisense RNA transcription*

Precedent studies have shown that antisense RNA-based strategies can be used to enhance mRNA degradation and consequently to interfere with protein biosynthesis in *E. histolytica* (Ankri *et al.*, 1998; Sahoo *et al.*, 2003; Vats *et al.*, 2005). *kerp1* gene was cloned in antisense orientation under the control of a tetracycline (Tet)-inducible promoter (see *Experimental procedures* for details). After electroporation of virulent wild-type HM1:IMSS trophozoites (WT) with either the original (pCTL) or recombinant (pAS) plasmids, transfectants were selected by hygromycin, subsequently controlled by PCR and, respectively, named 'CTL' and 'AS'; these parasites were cultured before experiments in the presence or not of Tet.

Detection of *kerp1* antisense RNA in the different strains under above-mentioned culture conditions was attempted in vain in repeated Northern blot assays using either oligomeric DNA or *in vitro* transcribed RNA probes. Nevertheless, strand-specific retrotranscription ('AS-RT' primer, see Table S1) allowed the exclusive quantification of *kerp1* antisense RNA by qRT-PCR ('AS-F' and 'AS-R' primers). As described in *Experimental procedures* for

other qRT-PCR, the experiment was repeated with two independent biological replicates, using two technical replicates performed in triplicates. As expected, no amplification was detected in the WT and CTL trophozoites, as well as in non-retrotranscribed samples of the AS strain. In contrast, in both retrotranscribed samples from the AS strain, antisense RNA was detected, indicating that it was transcribed in the absence and in the presence of Tet, a phenomenon probably due to a leaky activity of the promoter sequence. Antisense *kerp1* RNA relative abundance was normalized by the values obtained with *L9* mRNA. We arbitrarily set to 1 (with a standard deviation of 0.04) the normalized *kerp1* antisense abundance in the AS strain cultured without Tet. With Tet, this *kerp1* antisense RNA fragment was detected in equivalent amounts ( $1.18 \pm 0.39$ ;  $P > 0.05$ ). It is noteworthy that this method does not allow the identification of other RNA antisense molecules that do not carry the intact sequences we targeted with retrotranscription and PCR primers.

Then, we analysed the effect of antisense RNA on sense mRNA quantity and integrity. *kerp1* sense mRNA species were identified by Northern blot (Fig. 4A) and quantified by qRT-PCR (Fig. 4C) in WT, CTL and AS trophozoites. The Northern blot analysis was performed on total RNA purified from transfected and WT parasites; the oligomeric DNA probes used for hybridization were designed to detect only sense-oriented *kerp1* transcripts (see Table S1 for probe sequences). For all trophozoites, a single band of about 650 nucleotides, corresponding to *kerp1* mRNA, was identified. In addition, a second RNA band of roughly 400 nucleotides was detected in the AS strain, whose intensity was higher in the presence of Tet (Fig. 4A). The specificity of the probes indicates that the short mRNA species derived from *kerp1* gene transcription.

Nevertheless, to be freed from any doubt, we performed qRT-PCR assays that allowed highly specific differential detection and relative quantification of full-length and short mRNA species. As CTL and AS plasmids do not carry the 5'-untranslated regions (UTR) and 3'-UTR sequences of *kerp1* gene, we first identified by RACE these regions that flank *kerp1* coding sequence; they were then used for exclusive quantification of endogenous, sense mRNA species (refer to scheme drawn in Fig. 4B). To this goal, two different primers were used for retrotranscription: one straddling the 3'-UTR and the end of the coding sequence (*kerp1*-RT-2), and the other within the coding sequence (*kerp1*-RT-3). In all cases, sense mRNA was amplified using a forward primer overlapping the 5'-UTR and the beginning of *kerp1* coding sequence (*kerp1*-Q-F-2), thus preventing potential contamination by DNA sequences contained in the plasmid. Altogether, the data showed that there was no significant difference in *kerp1* full-length mRNA (retrotranscribed with *kerp1*-RT-2) quantities among the different strains and conditions

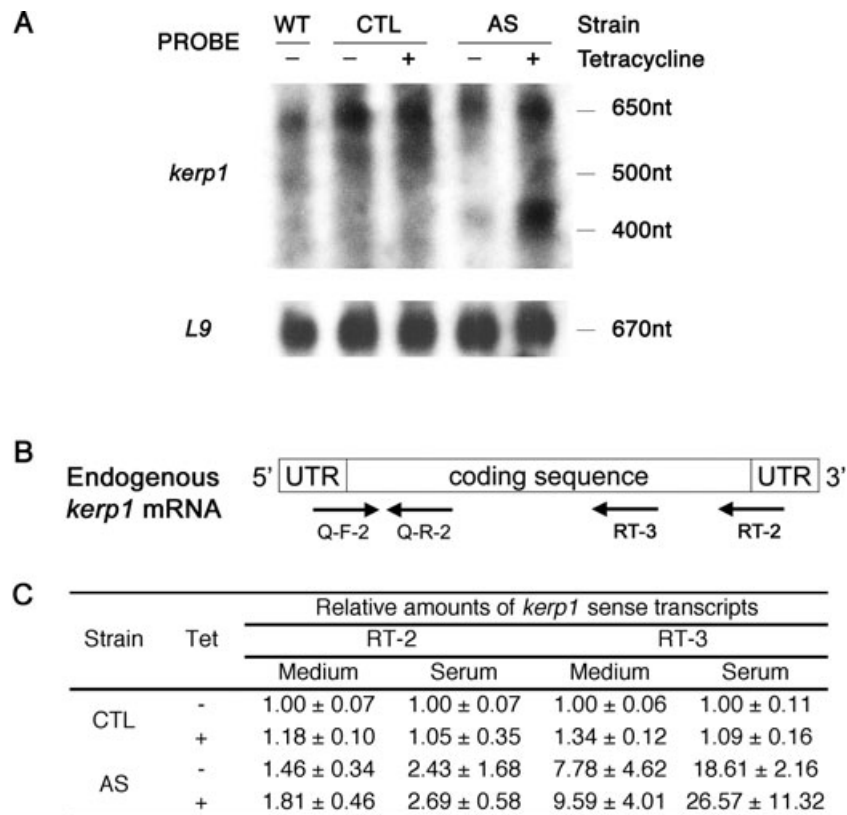


**Fig. 4.** Transcription of *kerp1* in modified strains.

A. Northern blot analysis of total RNA purified from WT, CTL and AS parasites. After electrophoresis of RNA and blotting, membranes were hybridized with probes complementary to *kerp1* or *L9* sense mRNA, allowing identification of sense transcripts. No significant difference was observed for the full-length *kerp1* mRNA, while a second band of lower size was detected in AS strain. nt, nucleotides.

B. The scheme depicts the strategy used for RNA quantification. The box represents the endogenous *kerp1* mRNA (gene ID number at NCBI: 3407934). Total RNA from WT, CTL, AS strains growing in the presence (or not) of Tet was submitted to retrotranscription and qRT-PCR as described in *Experimental procedures*. To detect sense RNA purified from WT, CTL, AS strains growing in the presence (or not) of Tet species, reverse transcription was performed with RT-2 (from +543 nt and covering the 10 first nucleotides of the 3'-UTR) or RT-3 (from +496 to +519 nt) primers. Then, qRT-PCR was carried out using Q-F-2 (covering the 7 last nucleotides of the 5'-UTR to +18 nt) and Q-R-2 (from +121 to +145 nt) primers.

C. Quantification of *kerp1* transcripts by qRT-PCR from total RNA purified from CTL and AS parasites. Raw data were normalized with respect to the abundance of *L9* mRNA; relative concentrations were calculated as described in *Experimental procedures*. Then, these were reported to the results obtained with the CTL strain without Tet. The abundance of *kerp1* full-length mRNA did not vary among strains and conditions. Detection of truncated sense-oriented *kerp1* mRNA (retrotranscribed with RT-3 primer) differed from CTL trophozoites and the AS strain, where it was increased. Data are the means of the results ± standard deviation) obtained with two matrix dilutions for two independent experiments ( $n = 4$ ), quantified in triplicate wells.

(Fig. 4C). In contrast, sense-oriented RNA retrotranscribed with *kerp1*-RT-3 (hybridizing to both mRNA types) was detected in higher amounts in AS trophozoites in the absence of Tet (7.78-fold increase referred to CTL,  $P = 0.022$  and 5.52-fold increase referred to CTL + Tet,  $P = 0.012$ ) and in the presence of Tet (9.59-fold increase compared with CTL;  $P = 0.009$ ; 7.17-fold increase compared with CTL + Tet;  $P = 0.007$ ); this primer allowed retrotranscription of both full-length and short *kerp1* sense RNAs. By comparing the data obtained in different strains and conditions, we thus concluded that along with the full-length *kerp1* mRNA, a truncated sense-oriented RNA is present in the AS strain and that its quantity is enhanced by the Tet treatment. However, due to the regu-

lation of *kerp1* gene expression during abscess formation (Figs 1 and 2), we were wondering whether the effect of antisense production was specifically revealed in infectious conditions. As classic virulence assays consist in injecting trophozoites into the portal vein of hamsters, we incubated the parasites in 70% non-heat-inactivated serum. Full-length and short sense mRNA species were then quantified by qRT-PCR as indicated above. In the presence of heat-inactivated serum (Fig. 4C), sense mRNA abundance was found not significantly modulated ( $P > 0.05$ ) but, surprisingly, the truncated form of sense mRNA was 18.61 times more abundant in the presence of serum without Tet and very highly overexpressed in the presence of serum and Tet (26.57-fold increase) as com-

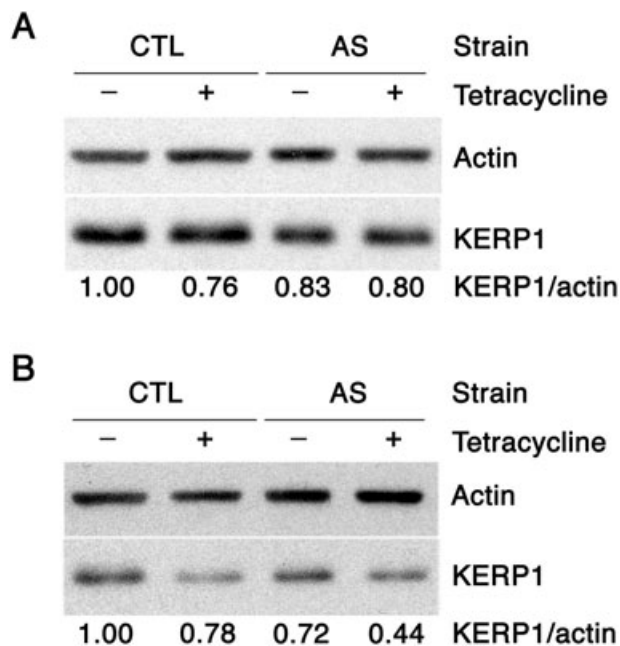


**Fig. 5.** KERP1 immunodetection in modified trophozoites. Trophozoites were incubated in axenic culture medium (A) or in the presence of 70% non-heat-inactivated serum (B). Crude extracts from  $2 \times 10^4$  trophozoites were loaded for each condition. KERP1 (25 kDa) and actin (43 kDa) were revealed with specific antibodies. Their relative abundance was determined as described in *Experimental procedures*. The detected amount of KERP1 is equivalent among strains during *in vitro* culturing. A decrease of KERP1 abundance was observed when parasites were incubated with serum. Then, AS trophozoites grown with Tet exhibit 56% decrease in KERP1 amount in comparison with CTL amoebae cultured without Tet. Similar results were obtained in two independent experiments.

pared with the CTL strains with or without Tet (in all cases,  $P < 0.05$ ).

To investigate the influence of antisense RNA transcription on KERP1 level, total-protein extracts were submitted to Western blot analysis (Fig. 5). Quantification of detected KERP1 led to conclude that there was no difference in KERP1 levels among parasites grown in culture medium (Fig. 5A) with or without Tet. Interestingly, KERP1 level was greatly reduced in the AS strain grown with Tet and treated by serum (Fig. 5B). KERP1 quantity within AS trophozoites was 39% decreased in comparison with the same strain cultured without Tet, 43% less than the CTL strain grown with Tet and 56% lower than within CTL amoebae not treated with Tet. These data showed an effect, although not yet understood, of the *kerp1* antisense transcription in stress conditions on KERP1 amount.

#### *In vivo* virulence assay with modified parasites

To assess the role of KERP1 during abscess formation, hamsters were infected with AS trophozoites that were cultivated for 5 days in the presence of Tet. Controls were

performed by infection of animals with CTL amoebae treated in the same manner or with AS parasites grown without Tet. Hamsters infected with trophozoites cultured with Tet drank water containing Tet before and during the period of infection. After 7 days, hamsters were sacrificed for pathophysiology analysis. Three independent experiments were performed. A total of 15 hamsters were inoculated for each condition (Table 3). Infection with AS parasites, grown in the absence of Tet, provoked the formation of liver abscesses quantitatively and qualitatively similar to those obtained with the CTL strain grown in the presence of Tet. For both these conditions, infection indices were consistent with previous results obtained with WT trophozoites. In contrast, a dramatic reduction of pathogenicity was observed with AS trophozoites grown in the presence of Tet, as these were inhibited for liver abscesses development. Indeed, in nine hamsters over 15 (60%), we did not macroscopically detect liver abscesses as compared with control conditions. Moreover, only three animals developed small liver abscesses in more than two lobes. These data showed that the induction of *kerp1* antisense RNA transcription accounted for inhibition of important pathogenicity features such as liver abscess onset.

#### Discussion

In most cases, colonization of the human colon by *E. histolytica* is either controlled by the host or even not detected; trophozoites appear to possess mechanisms for evading the human immune response (Campos-Rodriguez and Jarillo-Luna, 2005). For reasons that are yet to be well defined, amoebiasis is initiated when formerly commensal *E. histolytica* invades human tissues (such as the intestine or the liver). The occurrence of invasive amoebiasis in humans leads to environmental changes that impede para-

**Table 3.** *In vivo* virulence assay with modified strains.

Strain	Tet	Number of animals			Total
		Infection indices			
		0	1	2	
CTL	+	2	7	6	15
AS	-	1	4	10	15
	+	9	3	3	15

Seven days after infection with  $10^6$  trophozoites, hamsters were sacrificed, their livers were macroscopically observed and classified according to an infection index chart into three groups: no abscesses (0), one to three lobes with abscesses (1) and three to five lobes with confluent lesions (2). Fifteen animals were used in each experimental condition (five animals by experiment and a total of three experiments for each condition). Data were submitted to a  $\chi^2$  test and the results obtained with the Tet-treated AS strain were significantly differently distributed as compared with both other populations ( $P < 0.05$ ).

site encystation and trigger cell death in the host, leading to a shorter life span for both protagonists in the pathology unless they undergo dramatic changes in their shape, metabolism, signalling and overall gene expression patterns. Nonetheless, the question of how the virulence traits, i.e. the capacity to cause host damage or disease, of *E. histolytica* are positively selected is essential, as these traits guide the parasite into a dead end.

The host and parasite factors involved in the establishment of invasive amoebiasis have not yet been identified. It is believed that disease begins with the adherence of trophozoites to mucus and enterocytes via the Gal/GalNAc lectin, followed by lysis of the intestinal barrier by amoebic toxic factors (such as cysteine proteases), phagocytosis of host cells and an ensuing inflammatory response (Stanley, 2003). All these phenomena have been defined as *E. histolytica* virulence traits, despite the fact that precise reports of their action during the development of amoebiasis are rather scarce. Now that the *E. histolytica* genome has been sequenced (Loftus *et al.*, 2005) and that pioneer works concerning its transcriptome have been achieved (MacFarlane *et al.*, 2005; Gilchrist *et al.*, 2006; Weber *et al.*, 2006; Davis *et al.*, 2007), we expect that research based on comparative genomics, transcriptomics and proteomics will lead to a deeper understanding of the parasite's biology, its relationship with the host, the molecular mechanisms of immunopathology in amoebiasis and the development of innovative interventional strategies.

Based on the observation that axenic culture of *E. histolytica* reduces virulence (i.e. the parasite's ability to produce liver damage), we compared the gene expression of highly virulent and avirulent trophozoites from the same strain. To this end, we performed a transcriptome analysis with an oligonucleotide-based microarray designed according to information from *E. histolytica* transcripts. The first important finding was the observation of a stress response in virulent parasites. For instance, the stress-inducible gene *ssp1* was highly overexpressed. This factor had been previously identified due to its expression during adaptation of *E. histolytica* cells to stress conditions, such as heat shock (Weber *et al.*, 2006) or oxidative stress. Along with the *ssp1* gene, other upregulated genes were those encoding Hsp90 chaperone and peroxiredoxin; the latter is a surface molecule shown to protect *E. histolytica* against reactive oxygen species like H<sub>2</sub>O<sub>2</sub> (Choi *et al.*, 2005). Interestingly, a recent publication demonstrated that increased expression of peroxiredoxin in the non-virulent Rahman strain of *E. histolytica* increased virulence (Davis *et al.*, 2006) – an observation that supports our microarray results.

The second important finding was that genes encoding so-called 'classic' virulence factors were not upregulated in virulent trophozoites. In fact, some factors expected to be involved in the onset of liver abscess formation (such

as isotypes of the three Gal/GalNAc lectin subunits, the amoebapores A and C and cysteine proteinase 6) were even found to be somewhat downregulated. These data indicate either that the concentration of these factors may only increase under full-blown disease conditions or that their levels in cultured virulent parasites are already high enough to sustain pathogenic activity. The answer to this question is still pending. However, the gene encoding an asparagine-rich, *E. histolytica*-specific protein of unknown function called ARIEL was found to be upregulated, thus opening up opportunities for the study of this factor in virulence.

We performed an in-depth bioinformatics analysis (notably using PFAM and InterProScan) in an attempt to annotate and/or define specific protein domains. This approach enabled us to identify a group of lysine-rich protein-encoding genes (*krip* and *kerp*), which were upregulated in virulent trophozoites. The four putative KRiPs present signal peptides. Interestingly, *kerp1* (a gene encoding a protein that we had already studied with respect to parasite adherence to host cells) was found here to be upregulated in virulent trophozoites. We took advantage of a previous proteomic analysis performed on *E. histolytica* and identified KERP1, KERP2, KRiP2 and KRiP3 associated with phagosomes (Marion *et al.*, 2005). A qRT-PCR assay confirmed the upregulation of the *krip2*, *krip3*, *ariel* and *kerp1* genes already highlighted by microarray analysis.

To initiate studies allowing to decipher the role of these factors in pathogenesis, we chose KERP1 due to its involvement in parasite adhesion (Seigneur *et al.*, 2005), a major feature of *E. histolytica* virulence. The increase in *kerp1* expression in virulent parasites observed in our microarray study prompted us to examine whether this protein was an infection marker. In order to measure *kerp1* gene expression *in vivo*, we performed qRT-PCR with molecular beacons. The specificity of these particular oligonucleotide probes authenticates the amplified sequence, while their exceptional signal-to-background noise ratio allows accurate estimation of the quantity of amplicon. Optimization of this method for *kerp1* mRNA quantification in infectious conditions pushed the detection limit for a transcript in a pool of contaminants, as RNA species from trophozoites are greatly outnumbered by host cell RNAs. Here, for the first time, the abundance of a given *E. histolytica* mRNA was monitored throughout the course of infection in a reliable, quantitative manner. We observed that *kerp1* gene transcription is downregulated at the start of infection and then upregulated from the third day post infection. The pattern of *kerp1* mRNA abundance during the formation of liver abscesses highlighted a significant change in gene expression during the early periods (i.e. before 5 days) of infection. Thus, the pattern of *kerp1* mRNA abundance, which was increasing during the devel-

opment of massive abscesses, highlighted the intricate regulation of this gene and reinforced the data obtained by microarray analysis. Histoimmunochemical *in situ* analysis of the KERP1 protein revealed its increased detection from the third day post infection, indicating that KERP1 marked the progress of infection. However, considering that the decrease in *kerp1* mRNA at 3 days post infection does not directly correlates with protein levels observed in histology, we suggest that post-transcriptional features may regulate *kerp1* gene expression and that these account for the increase of protein abundance. Moreover, we cannot exclude that KERP1 concentrates in cortical areas of the cell from 2 days post infection, making it more detectable by the method we used. Knowing that the trophozoites' ability to induce liver abscesses is lost during axenic culture, we quantified KERP1 in amoebae at different time points after harvesting them from liver abscesses. The data showed a decrease in KERP1 abundance during axenic culture and lower amounts of KERP1 in trophozoites that had lost their ability to induce liver abscesses in the hamster model. These findings highlight the link between KERP1 and pathogenicity in *E. histolytica*.

In an attempt to investigate the direct involvement of KERP1 in pathogenicity, we submitted to *in vivo* virulence assays parasites modified for KERP1 production by an antisense strategy. The phenotype of these parasites suggests a singular regulation of *kerp1* gene transcription and transcript stability revealed by the presence of a second sense-oriented RNA specie of lower size, along with production of an antisense construct. Real alteration of protein concentration was only observed when AS trophozoites underwent a stress. Most of the mechanisms of gene transcription downregulation have been shown to involve the production of RNA molecules such as small interfering RNAs (siRNAs) of about 22 nucleotides, or the formation of double-stranded RNA hybrids (dsRNA), which can be cleaved in short RNA species then blocking protein translation. Efficient downregulation of gene expression has been obtained in *E. histolytica* by both siRNA treatment (Vayssie *et al.*, 2004) and dsRNA formation (Kaur and Lohia, 2004). In addition, antisense strategies have provided the opportunity to describe gene expression blockage in several cases (Ankri *et al.*, 1998; Sahoo *et al.*, 2003; Vats *et al.*, 2005) while the mechanisms they triggered remain still unknown. At this point, the molecular mechanism by which *kerp1* RNA species present in the AS strain cultured with Tet downregulate KERP1 production is still unknown. However, the data we report here combined with those recently obtained by Anbar *et al.* (2005) highlight the interference with gene expression and the original stability of the sense-oriented truncates of targeted mRNAs and also suggest that they might have a role to play in regulating amoebic gene expression. An hypothesis that needs careful analysis as short sense-oriented mRNA is also

present in the AS strain cultured without Tet where KERP1 abundance is invariant as compared with the CTL strain. These observations suggest that truncated mRNA specie may not directly be involved in the diminution of KERP1 abundance but may rather be one of the product of the full-length RNA degradation. A working hypothesis would be that *kerp1* antisense RNA transcription lead to a shorter life span of the full-length messenger, resulting, below a certain threshold reached in stress conditions for the AS strain growing with Tet, to an interference with protein translation. A feedback regulatory phenomenon may then enhance transcription of *kerp1* gene, hence the invariant quantified levels of full-length mRNA along with the increase of truncated sense mRNA. However, this unknown mechanism led to a significantly lowered pathogenicity in the hamster model, indicating that preservation of *kerp1* gene expression pathway integrity is important for the onset of liver abscess.

KERP1 was first identified for its capacity to interact with the brush border of enterocytes (Seigneur *et al.*, 2005). Its localization at the plasma membrane during liver abscess formation suggested that the protein was involved in the interaction between trophozoites and their environment. Moreover, KERP1 does not share any sequence homologies with other proteins and the lack of signal peptide in KERP1's sequence raised the question of its specific localization, as observed by *in situ* histoimmunochemistry. KERP1 may interact with other factors that mobilize it to the plasma membrane, and the identification of these hypothetical interacting molecules will shed light on the mechanisms involved in KERP1 trafficking. Furthermore, KERP1 is now characterized as a marker of the parasite invasion progression and as a virulence factor. There are several factors intervening early in amoebic liver infections that may influence KERP1 regulation directly such as nitric oxide, reactive oxygen species or cytokines production, or indirectly through the induction of stress response. Considering these facts and the presence of KERP1 at the parasite's surface, our working hypothesis is that KERP1 should play a role in protecting trophozoites from blood antimicrobial components and/or from acute immune response during liver abscess development and especially in interactions between trophozoites and host immune cells. Thus, understanding the role of KERP1 in pathogeny onset and development may help to decipher the role(s) played by factors from the KRiP family.

In conclusion, expression profiling of *E. histolytica* enabled us to explore the molecular features of the parasite's gene expression as a function of its infective capacity. The study provided insights into the transcriptional regulatory mechanisms that influence *E. histolytica*'s life cycle and infective status. Characterizing the molecules identified here should (i) provide information on the nature of the interactions that define the parasite–environment

system that efficiently sustains amoebiasis and (ii) open up unprecedented opportunities for diagnosing and controlling this human infectious disease.

## Experimental procedures

### *Entamoeba histolytica* culture

The axenic *E. histolytica* strain HM1:IMSS was cultured in TYI-S-33 medium at 37°C (Diamond, 1961). To obtain highly virulent trophozoites, the HM1:IMSS strain was inoculated into hamsters according to the published method (Rigotherier *et al.*, 2002). For axenization, parasites isolated from liver abscesses were grown in TYI-S-33 medium supplemented with 1.5 g l<sup>-1</sup> sodium sephotaxim (#3307093, Aventis) for 1 week. Transfected parasites were maintained in culture with 10 µg ml<sup>-1</sup> hygromycin B (#10687-010, Invitrogen).

### Hepatic inoculation procedure

Animal handling and experimentation were conducted according to the European Union- and the Pasteur Institute-approved protocols. Four-week-old male Syrian golden hamsters (*Mesocricetus auratus*), with a weight ranging from 90 to 100 g, were inoculated by the intraportal route with 10<sup>6</sup> HM1:IMSS trophozoites. For KERP1 functional test with Tet-treated parasites, drinking water provided to the animals was supplemented with 50 µg ml<sup>-1</sup> Tet for 48 h before inoculation and during the entire infection procedure. Five animals by experiment and conditions were used; in total, 45 hamsters were included in this evaluation. Treatment of animals and surgical procedures were performed according to the method of Tsutsumi *et al.* (1984). From 1 to 7 days post infection, hamsters were sacrificed, livers removed and treated either for RNA purification or for histological analysis.

For microarray experiments, after 7 days post infection, pieces of infected liver were incubated in TYI-S-33 medium and parasites were allowed to adhere to the culture tube for 16 h. Liver tissue was then discarded and RNA was purified from parasites. We recovered the totality of infected liver tissues coming from four hamsters in each biological replicate.

For histological analysis, dissected livers were photographed and inspected for the presence of amoebic abscesses, then fixed in 4% formaldehyde PBS (pH 7.4) and embedded in paraffin. Serial 5 µm sections were deparaffinized and treated for histoimmunocytochemistry as published (Rigotherier *et al.*, 2002) with a rabbit polyclonal antibody (1:50 dilution) raised against two peptides from KERP1 (H<sub>2</sub>N-CKSKGKGDIFYEN-COOH and H<sub>2</sub>N-KKQRLNDENNDCC-CONH<sub>2</sub>). Once incubated with the primary antibody, sections were washed three times in PBS, incubated with an anti-rabbit immunoglobulin G (1:100 dilution) coupled to horseradish peroxidase (#P0160, Dako) and further processed as previously described (Rigotherier *et al.*, 2002).

### RNA purification from trophozoites in axenic culture

Two or 10 million trophozoites in axenic culture were rinsed twice in PBS at 37°C and treated, respectively, with 2 or 6 ml of TRIzol reagent (Invitrogen). Quality and integrity of purified RNAs was checked by spectrophotometry at 230, 260, 280 and 320 nm,

electrophoresis on 0.8% agarose gel and assay on Bioanalyser 2100 (Agilent).

In case of incubation of parasites in the presence of serum, prior to RNA purification, 25 cm<sup>2</sup> culture flasks were filled with 25 ml of PBS, incubated for 30 min at 37°C, then 15 min at 37°C with 25 ml of 70% non-heat-inactivated adult bovine serum (#B11-011, PAA laboratories) in PBS.

### Synthesis of cDNA and microarray hybridization

A mixture of specific mRNAs (7.5 ng) from *Arabidopsis thaliana* [Spotreport mRNA Spikes, CAB (#252201), rbcL (#252203), LTP4 (#252204), LTP6 (#252205), XCP2 (#252206), RCP1 (#252207), TIM (#252209), PRKase (#252210), Stratagene] was mixed with 5 µg of *E. histolytica* RNAs. *A. thaliana* mRNAs were added at different dilutions in order to introduce a linear hybridization standard onto the microarray. The RNA mixture was retrotranscribed and labelled as previously described (Weber *et al.*, 2006) and then microarrays were hybridized. After drying by centrifugation, slides were scanned (GenePix 4000 A scanner, Axon) and images were analysed (GenePix5 software, Axon). The photomultiplier (PMT) gains were set to 480/450 (635 nm) and 430/400 (532 nm) for all slides. For each spot, the fluorescence value corresponded to the median pixel intensity within the spot (the GenePix F635 and F532 median columns). Three independent biological replicates were carried out in the experiment. For two of them two additional technical replicates were performed. Moreover, a dye swap was performed for each technical replicate to compensate biases introduced by the use of Cy3 and Cy5. Therefore, the experiment finally yielded 10 hybridized slides.

### Statistical analysis of microarray data

For normalization and differential analysis, scripts written with R software (<http://www.r-project.org>) were used. For normalization purposes, 1152 spots (corresponding to 24 seventy-base oligonucleotides designed on eight *A. thaliana* genes) were also spotted onto the microarray (Weber *et al.*, 2006). As spikes accounted for 37.5% of the total number of spots, Lowess normalization (Yang *et al.*, 2002) was performed on all spots (*Entamoeba* probes and spikes) with a slide-by-slide basis (BioConductor package *marray*; <http://www.bioconductor.org>). After pooling data from technical and biological replicates, differential analysis was carried out using the VM method from the VarMixt package (Delmar *et al.*, 2005), with the Benjamini and Yekutieli *P*-value adjustment method (Reiner *et al.*, 2003). Empty and flagged spots were excluded; genes with at least nine raw values were analysed. After pooling data from technical and biological replicates, differential analysis was carried out by paired Student's *t*-test using the variance estimating method: VM, from VarMixt package (Delmar *et al.*, 2005). The raw *P*-values were adjusted by the Benjamini and Yekutieli method (Reiner *et al.*, 2003), which controls the false discovery rate (FDR). We considered as being differentially expressed the genes with a Benjamini and Yekutieli *P*-value < 0.05 and expression fold change ≥ 2. An expression threshold, i.e. the mean of empty spots intensity plus two standard deviation, was calculated on each slide. Probes with intensity under the threshold on all slides were considered as low expression probes and eliminated from the final list of differentially expressed genes. The complete data set is available in Tables S2

and S3; detailed analyses are in addition available at <http://genoscript.pasteur.fr>. Click on public area, select *Entamoeba* link, experiment *virulent\_2* and search for significant results. Data can be ordered by ratio, gene name, FDR or other displayed columns.

### Retrotranscription

Purified RNAs were retrotranscribed with Superscript II Retro-Transcriptase (#18064-014, Invitrogen) according to manufacturer's protocol with specific primers listed as 'RT' (unless otherwise stated) in Table S1. In the same reaction mix was retrotranscribed each tested mRNA and the *L9* mRNAs (60S ribosomal protein *L9*-encoding gene loci 117.t00010, 117.t00014, 312.t00001, 465.t00004), which were used as endogenous normalizers as they were invariant in microarray experiments. This choice was supported by the comparison of *L9* and *L31* ribosomal protein gene expression levels in virulent and avirulent trophozoites, as the latter gene was also found invariant by the microarray analysis we performed.

### qRT-PCR and data analysis

After retrotranscription, qRT-PCR was carried out using an ABI Prism 7900HT system (Applied Biosystems). Reactions were performed in 20  $\mu$ l, which contained 500 nM of each primer, 1 $\times$  PCR SYBRGreen Master Mix (#4309155, Applied Biosystems) and 5  $\mu$ l of template cDNA. Primers used for amplification are listed in Table S1 as 'Q-F' and 'Q-R', 'Q-F-2' and 'Q-R-2' or 'AS-R' and 'AS-R'. A control curve using serial 10-fold dilutions of cDNA in water was used to validate amplification efficiency. After initial denaturation for 10 min at 95°C, the amplification cycle (repeated 40 times) was as follows: 15 s at 95°C, 15 s at 55°C and 15 s at 60°C. Then, a denaturation curve (55°C to 95°C, 2°C min<sup>-1</sup>) allowed to check if a unique amplicon was produced.

Threshold cycles (Ct) obtained for each sample well (supporting a standard deviation lower than 0.6 within the triplicates) were submitted to regression using the linear standard plot obtained with cDNAs from control trophozoites in axenic culture as a reference (outlined in ABI Prism 7700 Sequence Detection System Bulletin # 2). For each triplicate, the mean of the relative concentrations obtained for the tested mRNA were divided by the mean of the corresponding values obtained for *L9* mRNA, the chosen endogenous normalizer; this ratio represents the variation of the tested gene's mRNA abundance in the sample condition compared with the control condition. Data were retained when values obtained for two sequential dilutions fitted the control equation. Each PCR experiment was repeated twice, and the samples were prepared independently starting from the retrotranscription step. For each condition, means and standard deviations were calculated using the values kept after regression ( $n = 4$ ). Statistical analysis allowing the comparison of gene expression between different conditions was achieved by Student's two-tailed *t*-test or one-way ANOVA.

### RNA purification from infected livers and cDNA synthesis

Inflammatory foci were immediately excised from dissected livers and treated with TRIzol reagent (5 ml per liver). To disrupt

the tissues, 1.5 g of zirconia/silica and 1 g of zirconia beads (#11079101z and #11079110zx, BioSpec Products) were added to the sample subsequently vortexed thrice for 1 min. After centrifugation, the supernatants were transferred to another tube and the tissues treated once again with TRIzol reagent as previously mentioned. A first chloroform extraction was performed on the pooled supernatants and then the aqueous phase was submitted to another TRIzol-chloroform extraction, followed by isopropanol precipitation, DNase treatment (#2238, Ambion) and isopropanol precipitation.

After primer-specific retrotranscription (*kerp1*-RT and *L9*-RT, as listed in Table S1), cDNA was ethanol-precipitated, RNAs were degraded (#11119915001, Roche) and proteins and free nucleotides were removed by phenol-chloroform and subsequent chloroform extraction followed by ethanol precipitation.

### qRT-PCR using molecular beacons

Molecular beacons are oligonucleotidic probes with a stem-loop structure carrying a 5'-coupled fluorochrome and a 3'-coupled quencher. Fluorescence emission requires linearization of the molecular beacon, depending on its hybridization to its target, thus generating a very low background of fluorescence. Molecular beacons (listed as 'MB' in Table S1) were synthesized at the Pasteur Institute Oligonucleotide Synthesis Platform by coupling 2'-deoxyribonucleotides in 5' to 6-FAM and in 3' to Black Hole Quencher 1. Designed for qRT-PCR, these probes were first tested *in vitro* according to the following method. *kerp1* or *L9* targets were amplified in 20  $\mu$ l with 1 $\times$  AmpliTaq Gold Master Mix (#4316753, Applied Biosystems) using cDNA from trophozoites in axenic culture as matrices and 10  $\mu$ M primers (listed as 'Q-F' and 'Q-R' in Table S1). *kerp1* or *L9* molecular beacons were then added to a final concentration of 500 nM. The four reaction mixes (each molecular beacon with each target) were submitted to a denaturation step at 95°C for 10 min and a standard denaturation curve using the ABI 7900HT system. Fluorescence emission during the final denaturation (35°C to 95°C with a 2°C minute<sup>-1</sup> ramping) was then plotted as a function of the temperature (Fig. 1). We could then check the validity of the molecular beacons for both specificity and hybridization temperature to their targets. Using the ABI 7900HT system, the abundance of PCR-amplified cDNA (reported by molecular beacons) was quantified. Each well contained 20  $\mu$ l with 5  $\mu$ l of matrix and final 1 $\times$  AmpliTaq Gold Master Mix, 500 nM molecular beacon and 10  $\mu$ M of each primer ('Q-F' and 'Q-R' in Table S1). After retrotranscription, cDNA was re-suspended in an appropriate volume of water, which was determined by preliminary experiments, and serial 10-fold dilutions were performed. After initial denaturation at 95°C for 10 min, 50 amplification cycles (95°C for 15 s, 55°C for 30 s, 72°C for 15 s) were performed and fluorescence was measured during the hybridization step. A final dissociation curve was plotted after measuring fluorescence emitted between 35°C and 95°C with a 2°C minute<sup>-1</sup> ramping and allowed to confirm the amplification of the molecular beacons' specific target. Data were analysed as described above.

### Analysis of proteins by immunoblotting

Two million trophozoites were washed in PBS, harvested by shaking, centrifuged and re-suspended in a mixture of protease

inhibitors, SDS and Tris 10 mM (pH 7.4), to obtain a final concentration of  $4 \times 10^3$  amoebae  $\mu\text{l}^{-1}$ , 10 mM leupeptine (Sigma), 1 mM *N*-ethylmaleimide (Sigma), 2 mM *p*-chloromercuribenzoate (Sigma), 2 mM 4-(2-aminoethyl)benzenesulfonyl fluoride (Uptima), complete mini EDTA-free (protease inhibitor cocktail, Roche) and 1% SDS. Crude extracts were then boiled for 3 min at 100°C. In case of incubation of parasites in the presence of serum, prior to protein extraction, trophozoites were harvested, re-suspended in PBS at a concentration of  $10^4$  cells  $\mu\text{l}^{-1}$ , incubated for 30 min at 37°C, then 15 min at 37°C with 70% non-heat-inactivated adult bovine serum (#B11-011, PAA laboratories) at a concentration of  $3 \times 10^3$  cells  $\mu\text{l}^{-1}$ .

Protein samples, corresponding to an equivalent number of  $10^4$  trophozoites per well, were treated by immunoblotting (Towbin *et al.*, 1979) with the above-mentioned rabbit anti-KERP1 antibody (1:500 dilution) and with a mouse anti-actin monoclonal antibody (1:20 000 dilution; #69100, MP Biomedicals). Scanned autoradiographs were analysed by ImageQuant software (Molecular Dynamics), allowing quantification of light emission. Standard curves for KERP1 and actin abundance were made using serial dilutions of samples. These curves allowed to determine, by regression, relative concentration of proteins in each experimental condition. Comparison of KERP1 abundance between samples was thus possible using normalization by actin values.

#### Plasmid construction and transfection of parasites

Using specific primers ('cloning-F' and 'cloning-R' listed in Table S1), *kerp1* gene was amplified from genomic DNA of HM1:IMSS strain. Then, the PCR product was cloned into pCR2.1TOPO plasmid (Invitrogen) according to manufacturer's recommendations. The recombinant plasmid was purified and digested by *KpnI* restriction endonuclease. The resulting DNA fragment was ligated into pEhHYG-tetR-O-CAT vector (Hamann *et al.*, 1997) digested with the same restriction enzyme and the insert was cloned under the control of the Tet-inducible promoter. The antisense gene orientation was checked by endonuclease restriction and the recombinant plasmid was transfected into HM1:IMSS virulent trophozoites as previously described (Hamann *et al.*, 1997). Transfected strains were maintained in culture with  $10 \mu\text{g ml}^{-1}$  hygromycin B. Before experiments, transfected strains were cultured with  $30 \mu\text{g ml}^{-1}$  hygromycin B for 48 h, then supplemented, or not, with  $1 \mu\text{g ml}^{-1}$  Tet for 5 days.

#### Rapid amplification of cDNA ends (RACE)

Rapid amplification of cDNA ends (RACE) method was used to determine both *kerp1* mRNA 5'- and 3'-UTR sequences from total RNAs purified from axenically cultured HM1:IMSS trophozoites. Using the 5'-RACE system (#18374-058, Invitrogen) and *kerp1*-5RACE-1 as GSP1, *kerp1*-5RACE-2 as GSP2 and *kerp1*-5RACE-3 as GSP3, the 5'-terminus of *kerp1* mRNA was PCR-amplified by *Pfu* Turbo DNA Polymerase (#600250-52, Stratagene). For 3'-RACE, poly A<sup>+</sup> RNAs were retrotranscribed, as mentioned above, using RDM-polyT primer. The first PCR amplification was performed with RDM and *kerp1*-3RACE-1 primers. Then, the nested PCR amplification was achieved with RDM and *kerp1*-3RACE-2 primers. Amplicons were then cloned into pCR-BluntII-TOPO (Invitrogen) vector and sequenced (Genome Express).

#### RNA analysis by Northern blot

Samples (30  $\mu\text{g}$  of total RNA) were incubated for 10 min at 85°C in 18  $\mu\text{l}$  of 1 $\times$  MOPS buffer containing 50% formamide, 8% formaldehyde, 200 ng of ethidium bromide. After chilling, 2  $\mu\text{l}$  of loading buffer (40% glycerol, 10 mM EDTA, 0.25% bromophenol blue and 0.25% xylene cyanol FF) were added to the samples, which were subsequently resolved by electrophoresis on 2.5% agarose/7% formaldehyde gel in 1 $\times$  MOPS buffer. Upward transfer was performed in 20 $\times$  SSC buffer and nucleic acids were cross-linked onto the membrane (#10102, Ambion) by a 1200 mJ  $\text{cm}^{-2}$  UV pulse (Stratalinker, 1800, Stratagene). Pre-hybridization was performed at 50°C for 4 h in 5 $\times$  SSC buffer containing 5 $\times$  Denhardt's solution, 1% SDS, 200  $\mu\text{g ml}^{-1}$  RNA (#109223, Roche) and 100  $\mu\text{g ml}^{-1}$  DNA (#D7656, Sigma). For each target, two probes complementary to the mRNA were designed, named *kerp1*-probe-1, *kerp1*-probe-2, *L9*-probe-1 and *L9*-probe-2 respectively (Table S1). The synthetic oligodesoxyribonucleotidic 70-mers were labelled by psoralen-biotin, according to manufacturer's recommendations (#AM1480, Ambion).

Then, for each targeted mRNA, 100 ng of both denatured probes were added to the pre-hybridization solution and incubated at 50°C overnight. Non-isotopic detection was performed using BrightStar® BioDetect™ Kit according to manufacturer's recommendations (#AM1930, Ambion).

#### Acknowledgements

We would like to thank Marie Christine Rigother for her extensive help with the animal experiments, Sandrine Moreira for the help with genoscript and Musa Mhlanga for his advice with molecular beacons technology. This work is supported by a grant from the Pasteur-Weizmann Research Council.

#### References

- Anbar, M., Bracha, R., Nuchamowitz, Y., Li, Y., Florentin, A., and Mirelman, D. (2005) Involvement of a short interspersed element in epigenetic transcriptional silencing of the amoebapore gene in *Entamoeba histolytica*. *Eukaryot Cell* **4**: 1775–1784.
- Ankri, S., Stolarsky, T., and Mirelman, D. (1998) Antisense inhibition of expression of cysteine proteinases does not affect *Entamoeba histolytica* cytopathic or haemolytic activity but inhibits phagocytosis. *Mol Microbiol* **28**: 777–785.
- Asgharpour, A., Gilchrist, C., Baba, D., Hamano, S., and Houpt, E. (2005) Resistance to intestinal *Entamoeba histolytica* infection is conferred by innate immunity and Gr-1+ cells. *Infect Immun* **73**: 4522–4529.
- Campos-Rodriguez, R., and Jarillo-Luna, A. (2005) The pathogenicity of *Entamoeba histolytica* is related to the capacity of evading innate immunity. *Parasite Immunol* **27**: 1–8.
- Choi, M.H., Sajed, D., Poole, L., Hirata, K., Herdman, S., Torian, B.E., and Reed, S.L. (2005) An unusual surface peroxiredoxin protects invasive *Entamoeba histolytica* from oxidant attack. *Mol Biochem Parasitol* **143**: 80–89.
- Davis, P.H., Zhang, X., Guo, J., Townsend, R.R., and Stanley, S.L., Jr (2006) Comparative proteomic analysis of two *Entamoeba histolytica* strains with different virulence

- phenotypes identifies peroxiredoxin as an important component of amoebic virulence. *Mol Microbiol* **61**: 1523–1532.
- Davis, P.H., Schulze, J., and Stanley, S.L., Jr (2007) Transcriptomic comparison of two *Entamoeba histolytica* strains with defined virulence phenotypes identifies new virulence factor candidates and key differences in the expression patterns of cysteine proteases, lectin light chains, and calmodulin. *Mol Biochem Parasitol* **151**: 118–128.
- Delmar, P., Robin, S., and Daudin, J.J. (2005) VarMixt: efficient variance modelling for the differential analysis of replicated gene expression data. *Bioinformatics* **21**: 502–508.
- Diamond, L.S. (1961) Axenic cultivation of *Entamoeba histolytica*. *Science* **134**: 336–337.
- Gilchrist, C.A., Houpt, E., Trapaidze, N., Fei, Z., Crasta, O., Asgharpour, A., et al. (2006) Impact of intestinal colonization and invasion on the *Entamoeba histolytica* transcriptome. *Mol Biochem Parasitol* **147**: 163–176.
- Hamann, L., Buss, H., and Tannich, E. (1997) Tetracycline-controlled gene expression in *Entamoeba histolytica*. *Mol Biochem Parasitol* **84**: 83–91.
- Kaur, G., and Lohia, A. (2004) Inhibition of gene expression with double strand RNA interference in *Entamoeba histolytica*. *Biochem Biophys Res Commun* **320**: 1118–1122.
- Leippe, M. (1997) Amoebapores. *Parasitol Today* **13**: 178–183.
- Lidell, M.E., Moncada, D.M., Chadee, K., and Hansson, G.C. (2006) *Entamoeba histolytica* cysteine proteases cleave the MUC2 mucin in its C-terminal domain and dissolve the protective colonic mucus gel. *Proc Natl Acad Sci USA* **103**: 9298–9303.
- Loftus, B., Anderson, I., Davies, R., Alsmark, U.C., Samuelson, J., Amedeo, P., et al. (2005) The genome of the protist parasite *Entamoeba histolytica*. *Nature* **433**: 865–868.
- MacFarlane, R.C., and Singh, U. (2006) Identification of differentially expressed genes in virulent and nonvirulent *Entamoeba* species: potential implications for amoebic pathogenesis. *Infect Immun* **74**: 340–351.
- MacFarlane, R.C., Shah, P.H., and Singh, U. (2005) Transcriptional profiling of *Entamoeba histolytica* trophozoites. *Int J Parasitol* **35**: 533–542.
- Mai, Z., and Samuelson, J. (1998) A new gene family (ariel) encodes asparagine-rich *Entamoeba histolytica* antigens, which resemble the amoebic vaccine candidate serine-rich *E. histolytica* protein. *Infect Immun* **66**: 353–355.
- Marion, S., Laurent, C., and Guillen, N. (2005) Signalization and cytoskeleton. Activity through myosin IB during the early steps of phagocytosis in *Entamoeba histolytica*: a proteomic approach. *Cell Microbiol* **7**: 1504–1518.
- Petri, W.A., Jr, Haque, R., and Mann, B.J. (2002) The bitter-sweet interface of parasite and host: lectin-carbohydrate interactions during human invasion by the parasite *Entamoeba histolytica*. *Annu Rev Microbiol* **56**: 39–64.
- Ravdin, J.I., Murphy, C.F., Guerrant, R.L., and Long-Krug, S.A. (1985) Effect of antagonists of calcium and phospholipase A on the cytopathogenicity of *Entamoeba histolytica*. *J Infect Dis* **152**: 542–549.
- Reiner, A., Yekutieli, D., and Benjamini, Y. (2003) Identifying differentially expressed genes using false discovery rate controlling procedures. *Bioinformatics* **19**: 368–375.
- Rigothier, M.C., Khun, H., Tavares, P., Cardona, A., Huerre, M., and Guillen, N. (2002) Fate of *Entamoeba histolytica* during establishment of amoebic liver abscess analyzed by quantitative radioimaging and histology. *Infect Immun* **70**: 3208–3215.
- Sahoo, N., Bhattacharya, S., and Bhattacharya, A. (2003) Blocking the expression of a calcium binding protein of the protozoan parasite *Entamoeba histolytica* by tetracycline regulatable antisense-RNA. *Mol Biochem Parasitol* **126**: 281–284.
- Said-Fernandez, S., and Lopez-Revilla, R. (1988) Free fatty acids released from phospholipids are the major heat-stable hemolytic factor of *Entamoeba histolytica* trophozoites. *Infect Immun* **56**: 874–879.
- Salata, R.A., and Ravdin, J.I. (1986) Review of the human immune mechanisms directed against *Entamoeba histolytica*. *Rev Infect Dis* **8**: 261–272.
- Satish, S., Bakre, A.A., Bhattacharya, S., and Bhattacharya, A. (2003) Stress-dependent expression of a polymorphic, charged antigen in the protozoan parasite *Entamoeba histolytica*. *Infect Immun* **71**: 4472–4486.
- Seigneur, M., Mounier, J., Prevost, M.C., and Guillen, N. (2005) A lysine- and glutamic acid-rich protein, KERP1, from *Entamoeba histolytica* binds to human enterocytes. *Cell Microbiol* **7**: 569–579.
- Seydel, K.B., Li, E., Zhang, Z., and Stanley, S.L., Jr (1998) Epithelial cell-initiated inflammation plays a crucial role in early tissue damage in amoebic infection of human intestine. *Gastroenterology* **115**: 1446–1453.
- Stanley, S.L., Jr (2003) Amoebiasis. *Lancet* **361**: 1025–1034.
- Towbin, H., Staehelin, T., and Gordon, J. (1979) Electrophoretic transfer of proteins from polyacrylamide gels to nitrocellulose sheets: procedure and some applications. *Proc Natl Acad Sci USA* **76**: 4350–4354.
- Tsutsumi, V., Mena-Lopez, R., Anaya-Velazquez, F., and Martinez-Palomo, A. (1984) Cellular bases of experimental amoebic liver abscess formation. *Am J Pathol* **117**: 81–91.
- Tyagi, S., and Kramer, F.R. (1996) Molecular beacons: probes that fluoresce upon hybridization. *Nat Biotechnol* **14**: 303–308.
- Vats, D., Vishwakarma, R.A., Bhattacharya, S., and Bhattacharya, A. (2005) Reduction of cell surface glycosylphosphatidylinositol conjugates in *Entamoeba histolytica* by antisense blocking of *E. histolytica* GlcNAc-phosphatidylinositol deacetylase expression: effect on cell proliferation, endocytosis, and adhesion to target cells. *Infect Immun* **73**: 8381–8392.
- Vayssie, L., Vargas, M., Weber, C., and Guillen, N. (2004) Double-stranded RNA mediates homology-dependent gene silencing of gamma-tubulin in the human parasite *Entamoeba histolytica*. *Mol Biochem Parasitol* **138**: 21–28.
- Weber, C., Guigon, G., Bouchier, C., Frangeul, L., Moreira, S., Sismeiro, O., et al. (2006) Stress by heat shock induces massive down regulation of genes and allows differential allelic expression of the Gal/GalNAc lectin in *Entamoeba histolytica*. *Eukaryot Cell* **5**: 871–875.
- Yang, Y.H., Dudoit, S., Luu, P., Lin, D.M., Peng, V., Ngai, J., and Speed, T.P. (2002) Normalization for cDNA microarray data: a robust composite method addressing single and multiple slide systematic variation. *Nucleic Acids Res* **30**: e15.

Zhang, W.W., and Samuelson, J. (1993) The cDNA sequence of an abundant *Entamoeba histolytica* 20-kilodalton protein containing four repetitive domains. *Mol Biochem Parasitol* **60**: 323–326.

### Supplementary material

The following supplementary material is available for this article online:

**Table S1.** Oligonucleotide sequences of molecular beacons and primers used for retrotranscription, for PCR or as probes.

**Table S2.** Genes downregulated in virulent parasites. Listed are annotated genes that are significantly downregulated in

virulent trophozoites, regardless of the gene expression fold change.

**Table S3.** Genes upregulated in virulent parasites. Listed are annotated genes that are significantly upregulated in virulent trophozoites, regardless of the gene expression fold change.

This material is available as part of the online article from:  
<http://www.blackwell-synergy.com/doi/abs/10.1111/j.1462-5822.2007.01030.x>

Please note: Blackwell Publishing is not responsible for the content or functionality of any supplementary materials supplied by the authors. Any queries (other than missing material) should be directed to the corresponding author for the article.